Polymer 350 (2026) 129769

Contents lists available at ScienceDirect

Polymer

journal homepage: www.elsevier.com/locate/polymer

Silylation of lignin as an effective tool for the development of bio-based oil structuring materials

M. Trejo-Cáceres, J.E. Martín-Alfonso *, J.M. Franco

Department of Chemical Engineering and Materials Science, Campus de El Carmen, University of Huelva, Chemical Product and Process Technology Research Center (Pro²TecS), 21007, Huelva, Spain

ARTICLE INFO

Keywords:
Lignin
Silylation process
Bio-lubricant
Rheology
Friction and wear

ABSTRACT

In this work, silylation process was employed as straightforward approach to develop biolubricants based on kraft lignin. The silylation reaction was conducted using tert-butyldimethylsilyl chloride (TBDMSCl) in the presence of dimethylformamide and imidazole as solvent and catalyst, respectively. By adjusting reaction times (2-24 h), several levels of physicochemical modification were achieved. Structural analysis via FTIR and two-dimensional ^{1}H–^{13}C HSQC NMR spectroscopy confirmed the successful incorporation of silane groups into lignin chemical structure, improving wettability and dispersibility. Additionally, SEM revealed notable changes in lignin particle morphology, particularly in particle size and aggregation. These physicochemically modulable amphipathic particles, containing hydrophilic groups and hydrophobic silane segments, were incorporated into castor oil and significantly impacted the rheological and tribological properties of the oleo-dispersions. Two distinct rheological behaviours were observed: liquid-like (at low reaction times <5 h) and gel-like (at high reaction times, > 16 h), where the silane groups, which act as a "bridge" for interaction with castor oil, and the area/volume ratio of lignin particles played a key role. The anti-friction and anti-wear properties were excellent, similar to or better than those obtained with castor oil or traditional lithium lubricating greases, attributed to the mending effect of the silylated lignin particles. This work offers a fast and straightforward compatibilization strategy to produce sustainable oil structuring agents, particularly relevant in the lubricant industry.

1. Introduction

The development of new lubricant formulations has gained significant momentum due to their critical role in reducing parasitic frictional energy losses, improving the efficiency of power transmission and extending the life of mechanical components [1,2]. Friction is the major source of energy loss in moving parts. In particular, reducing friction is a key strategy in the pursuit of carbon neutrality, as approximately 20% of the world's primary energy generated annually is used to overcome frictional resistance [3]. In general, semi-solid lubricants (such as greases) are complex colloidal systems containing a thickener dispersed in either mineral or synthetic oil [4]. The thickener is usually a metallic soap produced by the saponification of fatty acids, although non-soap alternatives such as polymers can also be used [5]. This thickener forms a three-dimensional network that entraps the oil and gives the grease its desired rheological and tribological properties. These specific properties are influenced by the nature and concentration of the components, as well as the microstructure created during the manufacturing process [6]. This structure has a direct impact on the performance of the grease in different industrial applications, ensuring optimum lubrication under varying conditions.

Replacing traditional thickeners with more environmentally friendly alternatives presents greater challenges compared to replacing non-biodegradable lubricants with vegetable oils or their derivatives. This is because the thickener must create a suitable network that effectively traps the oil while also providing essential functional properties, such as physical, mechanical, thermal stability, and lubrication performance. Achieving this balance is crucial, as the thickener must ensure the lubricant performs well under varying conditions while being environmentally responsible. Within this context, the development of new thickeners or methods for producing sustainable semi-solid lubricants has become a highly relevant research topic with huge industrial implications. This is particularly meaningful from an economic, social and environmental perspective. Recently, the potential use of lignin - often considered a by-product - as a valuable chemical precursor for the development of lubricant additives and thickeners has been investigated

* Corresponding author.
E-mail address: jose.martin@diq.uhu.es (J.E. Martín-Alfonso).

https://doi.org/10.1016/j.polymer.2026.129769
Received 25 December 2025; Received in revised form 15 February 2026; Accepted 19 February 2026
Available online 20 February 2026

[7–12]. These early results are promising and suggest that lignin could play a significant role in developing more sustainable and cost-effective lubricants. This opens up exciting opportunities to improve both the performance and environmental credentials of lubricants.

Lignin is a highly branched polyphenolic macromolecule that is an essential component of the cell walls of primarily terrestrial plants. It is formed by polymerization of phenylpropane units, i.e. p-hydroxyphenyl (H), guaiacyl (G) and syringyl (S) [13,14], yielding versatile functional structures with variable dispersity and no extended sequences of regularly repeating units, depending on the botanical origin and extraction process [15]. Lignin offers numerous benefits in the development of semi-solid lubricants, as it exhibits good thermal and mechanical stability [16]. Its distinctive phenolic structure also makes it an effective antioxidant additive, helping to prevent the physico-chemical degradation of lubricating oils during operation [11]. Additionally, this amorphous macromolecule is the most abundant terrestrial aromatic polymer [17], and has long been considered a low-value by-product of the biorefining and pulping processes [18]. However, it presents a notable inherent drawback, primarily linked to its limited capacity to form stable gel-like dispersions in hydrophobic media. This issue arises due to the numerous hydroxyl groups (–OH) present in its chemical structure, which hinder its ability to be dispersed effectively in oil. Despite this, the presence of these –OH groups can also be advantageous, as they offer a potential platform for chemical modifications. By derivatizing and functionalizing these groups, it's possible to reduce the material's hydrophilic nature, enhancing its compatibility with oils and improving its physical stability. Several chemical modifications have been reported to improve the physical compatibility of lignin with oil media, including alkylation [10], amination [19], esterification [7], epoxidation [20] and functionalization with isocyanate groups [21]. These approaches are mainly focused on enhancing the physical interaction between lignin and oils. Zhang et al. synthesized lignin by microwave amination and found that the lignin modified with heteroatom-rich chemicals can increase the viscosity of polyethylene glycol and enhance its adsorption to the metal surface, resulting in improved lubrication performance [10]. Cortés Triviño et al. studied the influence of epoxidation conditions on the rheological properties of epoxidized kraft lignin in castor oil and found that the linear viscoelasticity functions are quantitatively affected by the epoxidation parameters. In general, lignins with higher epoxidation index show higher values of the small-amplitude oscillatory shear functions, which are indicative of better gel-strength due to a higher cross-linking density between the epoxidated lignin and castor oil [20]. Borrero-López et al. discussed the effects of chemical modification of wheat straw soda lignins with 1,6-hexamethylene diisocyanate and found that functionalized lignin was able to chemically interact with castor oil via urethane bonds, providing oleogels with suitable rheological properties [21]. Recently, Wu et al. prepared oleogels with chemical cross-links between lignin modified with (3-aminopropyl) triethoxysilane and (3-glycidyloxypropyl) trimethoxysilane, along with castor oil. They investigated the influence of the lignin content with a single degree of modification on the performance properties and found that functionalized lignin acted as an effective thickener, significantly enhancing antiwear and antioxidation properties [8]. However, to the best of our knowledge, no comprehensive work on the impact of the silylation process on the functional properties of lignin oleo-dispersions has yet been reported. We hypothesize that precise control over the proposed alkyl-silyation method could lead to efficient synthesis of tunable modified lignin with tailored oil structuring properties, as a result of the physical interaction between the modified polymer with grafted hydrophobic alkyl-siloxane segments, which will act as a “bridge”, and the oil, thus enhancing compatibility.

In this work, we present an effective tool for the development of sustainable oil structuring agents by chemical modification. This approach involves the lignin silylation to develop biolubricant formulations. The main objectives of this work were (i) to study the role of the alkyl-silylation process on the chemical, morphological, hydrophobic and surface properties of modified lignin and (ii) to explore the ability of the lignin produced with different degrees of chemical modification to structure castor oil by analyzing its rheological and tribological properties, aiming to advance a new generation of biolubricant formulations.

2. Materials and methods

2.1. Materials

Kraft lignin (KL, ≤3.6 wt % sulfur content and specified pH of 10-11 (3 wt % in water)) was purchased from Sigma-Aldrich (code 471003). It was selected as a model lignin because it is a lignin widely produced from the pulp and paper industry and biomass refineries, and therefore commercially available on a large scale. The purity and composition of this lignin was determined by Gendron et al. [22] in a previous work and the results are shown in Table 1. As can be seen, Kraft lignin has a low lignin content (60 wt %), and a high residual ash content (27.9 wt %). Hence, these results suggest that the Kraft lignin has not been purified after the extraction process.

Tert-butyldimethylsilyl chloride (TBDMSCl, Reagent grade, 97%), imidazole (ImH, ≥99%), *N,N*-Dimethylformamide (DMF, anhydrous, 99.8%), methanol (CH_3OH, anhydrous, ≥99.8%), ethanol (CH_3 CH_2OH, ACS reagent, ≥99.5%), acetone ($CH_3(OH)$ CH_3, ACS reagent, ≥99.5%), cyclopentanone (C_5H_8O, ReagentPlus grade, ≥99%) were purchased from Sigma-Aldrich. Castor oil (viscosity: 0.55 Pa s, density: 0.958 g/mL, at 40 °C) was provided from Guinama, (Spain) and stored at room temperature (23 °C) in a dark area. The fatty acid profile can be found elsewhere [23]. The commercial lithium lubricating grease Castrol Optipit (Castrol, Germany) was used as benchmark.

2.2. Synthesis of silylated lignin

The one-step heterogeneous silylation process was carried out using TBDMSCl as silylating reagent, DMF as solvent and imidazole as catalyst. From an experimental point of view in a typical procedure, 2.0 g portion of previously dried KL was mixed with 10 mL of DMF in a 100 mL round bottom flask at room temperature (≈23 °C) with constant stirring until complete dissolution of the lignin. Then, imidazole and TBDMSCl (2 equiv. with respect to lignin, respectively) were added and the effect of silylation time on chemical substitution was investigated by varying the reaction times from 2 to 24 h. The imidazole/KL mass ratio was chosen to ensure sufficient imidazole as an auxiliary base to neutralize the HCl formed during the reaction and to ensure completion of the reaction. After the required time, the modified KLs were filtered out and thoroughly washed with a mixture of water and methanol (80:20 by weight) in order to remove un-reacted TBDMSCl and formed imidazole chloride. Finally, the silylated kraft lignins, coded as Si-hour, were oven dried at 45 °C for 24 h. Each experiment was repeated three times to check the consistency of the results.

Table 1
Purity and composition of lignin.

Lignins (wt %)		Carbohydrates (wt %)		Others (wt %)	
ASL	5.20 ± 0.40	**G**	0.63 ± 0.03	**Ash**	27.9 ± 0.60
AIL	58.8 ± 1.30	**XMG**	1.27 ± 0.03	**Deg**	8.20 ± 0.20
		A	0.60 ± 0.02		
TL	60.0 ± 1.70	**TC**	2.50 ± 0.10	**TO**	36.1 ± 0.80

ASL: Acid Soluble Lignin, **AIL**: Acid Insoluble Lignin, **TL**: Total Lignin, **G**: Glucose, **XMG**: Xylose-Mannose-Galactose, **A**: Arabinose, **TC**: Total Carbohydrates, **Deg**: Degradation products identified by HPLC at the end of the acid hydrolysis based on the NREL protocol (presence of acetic and formic acids, traces of levulinic acid, hydroxymethylfurfural, and furfural), **TO**: Total others. Data from Gendron et al. [22].

2.3. Characterization of lignin and silylated samples

The Fourier transform infrared (FT-IR) spectra of samples were conducted to confirm the incorporation of silane group into the lignin using a typical KBr method with a JASCO FT/IR-4200 spectrometer after the samples were purged with nitrogen. Each sample was scanned 46 times at a resolution of 4 cm^{-1} over the wavenumber region of 4000–400 cm^{-1}. For the ^{1}H–^{13}C 2D HSQC NMR analysis, around 50 mg of lignin was dissolved in 700 μL of DMSO-d_6 (approx. 70 mg/mL) and analyzed using a Bruker Avance NEO 500 MHz NMR spectrometer equipped with a 5 mm BBFO probe with a Z-gradient. ^{1}H NMR spectra were acquired using a 90° pulse of 5.97 μs, a relaxation delay of 10 s, a spectral width of 9615.385 Hz, and an acquisition time of 3.40 s, with 32 scans accumulated. For ^{13}C NMR spectra, a 30° pulse of 3.3 μs was applied, with a relaxation delay of 2 s, a spectral width of 30120 Hz, an acquisition time of 1.09 s, and a total of 9000 scans. The ^{1}H–^{13}C HSQC spectra were recorded with spectral widths of 8196.72 Hz for ^{1}H and 20754.50 Hz for ^{13}C, collecting 1024 complex points in the proton dimension, with a relaxation delay of 1 s, 32 scans, and 256 time increments. The $^{1}J_{C–H}$ coupling constant was set at 145 Hz, with a J-coupling evolution delay of 1.72 ms. The DMSO peak at δ_C/δ_H 39.5/2.49 ppm ppm^{-1} was used for the calibration of the chemical shifts. NMR data were processed with MestreNova software (version 15.0.0, Mestrelab Research). The morphology of the samples was investigated by SEM imaging using a FlexSEM 1000 II electron microscope with an accelerating voltage of 5 kV with a 10 mm working distance after sputtering the samples with gold under vacuum. Thermogravimetric analysis (TGA) was conducted using a Q50 TGA model from TA Instruments (New Castle, DE, USA). The samples were placed in a platinum pan and heated within the temperature range from room temperature (25 °C) up to 600 °C at a heating rate of 10 °C/min under nitrogen flow (see the Supporting Information). To assess the hydrophilicity or hydrophobicity of the samples, 100 mg of samples were added to a 20 mL mixture of toluene and water (in a 1:1 ratio) and shaken vigorously. Since the solvents have opposite polarities, it was expected that the sample with hydrophilic properties would disperse primarily in the water phase (neat lignin), while the hydrophobic highly modified samples would remain in the toluene fraction, avoiding the water phase. The solubility of both lignin and silylated samples was also evaluated by dissolving 70 mg of the sample in 3 mL of organic solvent within conical tubes, using a vortex mixer to facilitate the process. Various organic solvents, including ethanol, acetone, and cyclopentanone, were tested, and the solubility of the samples was assessed through visual observation. Sessile-drop contact angle measurements were also performed using a dynamic goniometer to assess the hydrophobicity of the samples. This involved tracking the spreading behavior of a water droplet placed on the surface of both kraft lignin (KL) and silylated films. Apparent dynamic contact angles were determined by capturing side-view images of the droplet over time with a CCD camera (PixeLink PL-A741) and analyzing its shape profile. A droplet of deionized water (~5 μL) was carefully dispensed onto the sample surface at room temperature (~23 °C), and its spreading was quantified using axisymmetric drop shape analysis (ADSA-P). To prepare the sample films, materials were compressed under 1000 kPa for 25 s using a manual hydraulic press. Image analysis and contact angle measurements were carried out using FIJI ImageJ software (NIH, Maryland, USA).

2.4. Preparation of oleo-dispersions

Si-KL was incorporated into castor oil using a laboratory-scale mixing apparatus equipped with an anchor impeller. The process was carried out at ambient temperature (≈23 °C) with a rotation speed of 60 rpm for a duration of 1 h. The lignin concentration was set at 30 wt % according to previous work [7]. This method ensures a correct dispersion of the lignin in the oil medium.

2.5. Characterization of oleo-dispersions

The rheological properties of the oleo-dispersions were measured at 23 °C by using a stress-controlled rheometer (model Rheoscope, ThermoHaake, Germany). A rough parallel plate geometry of 20 or 35 mm diameter with 1 mm gap, depending on the sample, was used for both steady and oscillatory shear measurements to overcome the wall slip effects typically observed in these systems. For Small-Amplitude Oscillatory Shear (SAOS) tests, the stress sweep was completed at 6.28 rad/s to determine stress values within the linear viscoelastic regime. Frequency sweep tests were then performed from 0.03 to 100 rad/s at constant stress amplitude, well within the linear viscoelastic regime. Steady shear viscosity measurements were conducted between shear rates of 0.01 and 100 s^{-1}, with viscosity data collected every 3 min once the apparent viscosity had stabilized at the applied shear rate. All rheological measurements were performed in duplicate for each sample. If the replicates showed a difference greater than 5%, additional runs were performed as necessary, and outliers were removed.

The tribological properties of the oleo-dispersions were measured at 23 °C by using a rotational rheometer (Physica MCR-501, Anton Paar, Austria) equipped with a steel-steel ball-on-three-plates tribological configuration. Three plates (15 × 6 × 3 mm, 1.4301 AISI 304, 0.21 μm roughness, 80 HRB hardness) are arranged at an angle of 45° to center a 1/2″ diameter ball (1.4401 grade 100 AISI 316) and evenly distribute the normal load. While the plates remain stationary, the ball rotates at a given rotational speed. The steady-state coefficient of friction was determined at room temperature (23 °C) by applying a normal force of 20 N and a constant rotational speed of 100 rpm, within the mixed friction regime, until a steady-state value was reached (for ~650 s). The topography of the wear scar surface left in the steel plates by the constant rotational speed tests was examined by scanning electron microscopy (SEM) using a FlexSEM 1000 II electron microscope. Tribological measurements were repeated three times using fresh samples for each run.

3. Result and discussion

3.1. Influence of silylation process on properties of lignin

The one-step heterogeneous silylation process was carried out in this research using TBDMSCl as silylating reagent, DMF as solvent and imidazole as catalyst, as shown in Fig. 1a. Silylation of lignin involves the substitution of an alkyl silyl group for a hydroxyl group to form an alkylsilyl ether via an SN2 reaction mechanism [24,25]. This process occurs on both aliphatic and aromatic hydroxyl groups, as reported in previous studies [26,27]. On the other hand, silylation activation can proceed via two different catalytic pathways: (i) via the N-tert-butyldimethylsilylimidazole intermediate [28] and (ii) via the silylated DMF transient complex [29]. In the first way, the non-protonated nitrogen of the imidazole ring attacks the silicon atom, forming a highly electrophilic counterion (silylimidazole), which causes the chloride to leave the silylating reagent (see Fig. 1b). In the case of DMF catalysis, the departure of the electron density from the leaving group of the silicon atom, such as chlorine, makes the silicon partially positive and thus susceptible to attack by the oxygen of the carbonyl group, resulting in the departure of the chloride ion. This happens because the oxygen in the carbonyl group, which is more electronegative, becomes partially negative and nucleophilic. The result is a salt consisting of chloride ions and a positively charged transient complex (see Fig. 1c). Both reaction intermediates are then attacked by the hydroxyl groups of the monolignols that form lignin, which act as nucleophiles. As the nucleophilic groups of lignin bind to the silicon atom, the bond between the leaving group and the silicon atom is simultaneously broken, allowing the imidazole nitrogen to take the electron pair and become electronically neutral. Furthermore, the chloride produced during catalytic activation reacts with the hydrogen of the alcohol to form HCl and the final

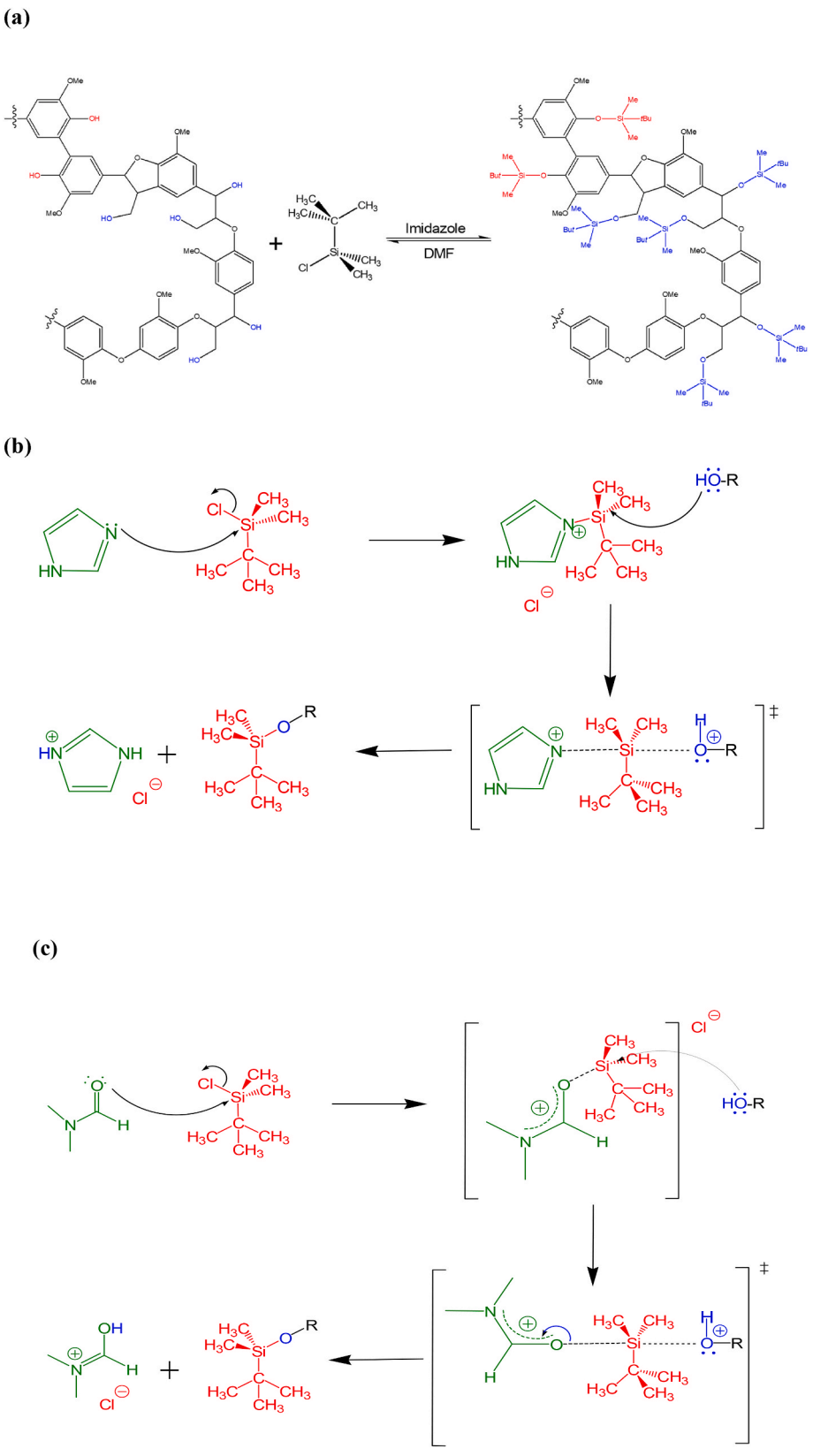

Fig. 1. (a) General mechanism of the silylation, (b) Catalysis mechanism via N-tert-butyldimethylsilylimidazole intermediate and (c) Catalysis mechanism via *N,N*-Dimethylformamide.

reaction product. Imidazole acts as a catalyst, remaining free at the end of the reaction, and functions as an auxiliary base to neutralize the HCl formed during the process. This results in the formation of a highly stable hydrochloride salt, which is difficult to recover [30,31], thereby requiring the use of excess imidazole.

FTIR was used to assess the chemical modification of KL after the silylation reaction, providing valuable insight into the structural changes. Fig. 2 displays the infrared spectra of both neat lignin and silylated samples as a function of reaction time. As can be seen, KL displays typical lignin bands. The broad absorption band at 3445 cm^{-1} is associated with the OH stretching vibrations of both aromatic and aliphatic OH groups, while the peaks between 2935 and 2845 cm^{-1} correspond to the vibrations of CH_3 and CH_2 groups. KL also displays typical aromatic skeletal vibrations at 1590, 1510 and 1415 cm^{-1}, as well as C–H deformation combined with aromatic ring vibration at 1450 cm^{-1} [32]. Notable absorption bands at 1265, 1225 and 1030 cm^{-1} are attributed to the guaiacyl (G) units, while the syringyl (S) units appear at 1130 cm^{-1}. As can be observed, the intensities of the peaks corresponding to the G units are significantly higher than those for the S units, indicating that KL contains a greater proportion of G units than S units. This reflects the nature of the feedstock, although the raw material from which Kraft lignin was derived remains unknown [33]. The spectra of the silylated samples confirm the successful silylation of KL. This is evidenced by the presence of characteristic silane bands, including one at 838 cm^{-1} corresponding to the Si–OH stretching vibration, another at 779 cm^{-1} associated with the Si–C and Si–O stretching vibrations and Si–O–Si stretching vibration at 1074 cm^{-1} [34,35]. Another change that supports the chemical modification of KL is the increase in intensity of the characteristic stretching vibration band for C–H (in $Si–CH_3$ at ~2935 and 2845 cm^{-1}) [36]. Furthermore, it is worth to mention that the silane band at 1257 cm^{-1}, corresponding to the $(C–H)_{silyl}$ in-plane bending of the methyl group, cannot be used to quantify the degree of chemical modification in these samples, as it overlaps with the G-unit band at 1265 cm^{-1}.

The kraft lignin and silylated samples were also characterized by 2D HSQC NMR to gain insights into the changes in structure, as well as in the linkages through chemical modification. The 2D HSQC NMR spectra of neat kraft lignin (Fig. S1) as well as the corresponding description and the assignment of the main $^{13}C–^{1}H$ correlation signals in the spectra (summarized in Table S1) are provided in the Supporting Information. To analyze the impact of the silylation process on the lignin structures, the 2D HSQC NMR spectra was divided into several distinct regions. Figs. 3 and 4 illustrate the regions corresponding to the aromatic (δ_H/δ_C 6.1-7.7/103-130 ppm) and non-oxygenated aliphatic (δ_H/δ_C −0.5-2/50-90 ppm) regions of the spectra, respectively. The oxygenated aliphatic region (δ_H/δ_C 2.5-5.5/50-90 ppm) has been included in the Supporting Information as Fig. S2. One possible way to assess the influence of the reaction time on the degree of chemical modification of silylated samples is by calculating the areas corresponding to the main lignin fraction structures. As the HSQC signal integrals were normalized with respect to aromatic units, the NMR-characterized silylation results can be directly related to these structural units. It should be noted that, while this normalization allows for relative spectroscopic comparisons between samples, it does not represent an absolute degree of substitution corresponding to a fixed number of hydroxyl groups per aromatic unit. The quantity of different areas was normalized using the following assumption [37]:

$$G + S = G_2 + S_{2,6}/2 = 100\,Ar \tag{1}$$

This assumption implies that the condensation (substitution) positions G_2 and $S_{2,6}$ of lignin is insignificant. However, it is still valuable for relative comparison with the literature data as this normalization is used when only HSQC spectra of lignins are available [38,39]. The results obtained are shown in Table S2 in the Supporting Information. As can be seen, these results confirm that reaction time is a key factor in the efficiency and type of structural modification occurring in lignin [40]. In the aromatic region (see Fig. 3), it is important to note that the S/G ratio remains constant at 0.1 throughout the process, indicating that the overall ratio between syringyl and guaiacyl units remains unchanged. This suggests that the silylation reaction is selectively directed to specific sites without significantly altering the overall aromatic composition of the lignin. In the case of the $S'_{2,6}$ units, they show a variable behavior,

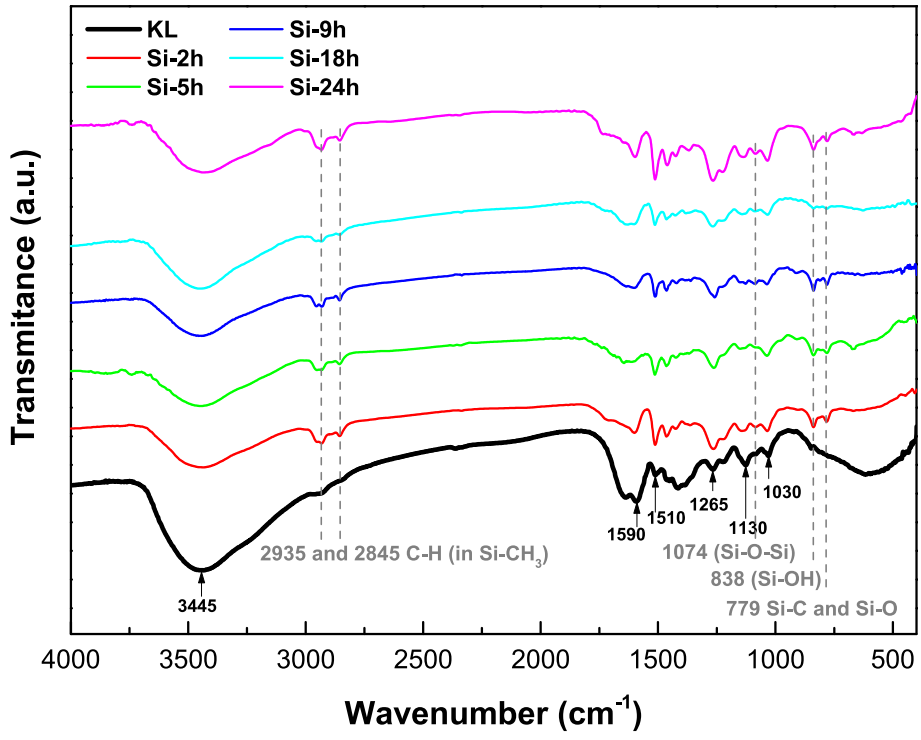

Fig. 2. FTIR spectra of KL and silylated samples as a function of reaction time.

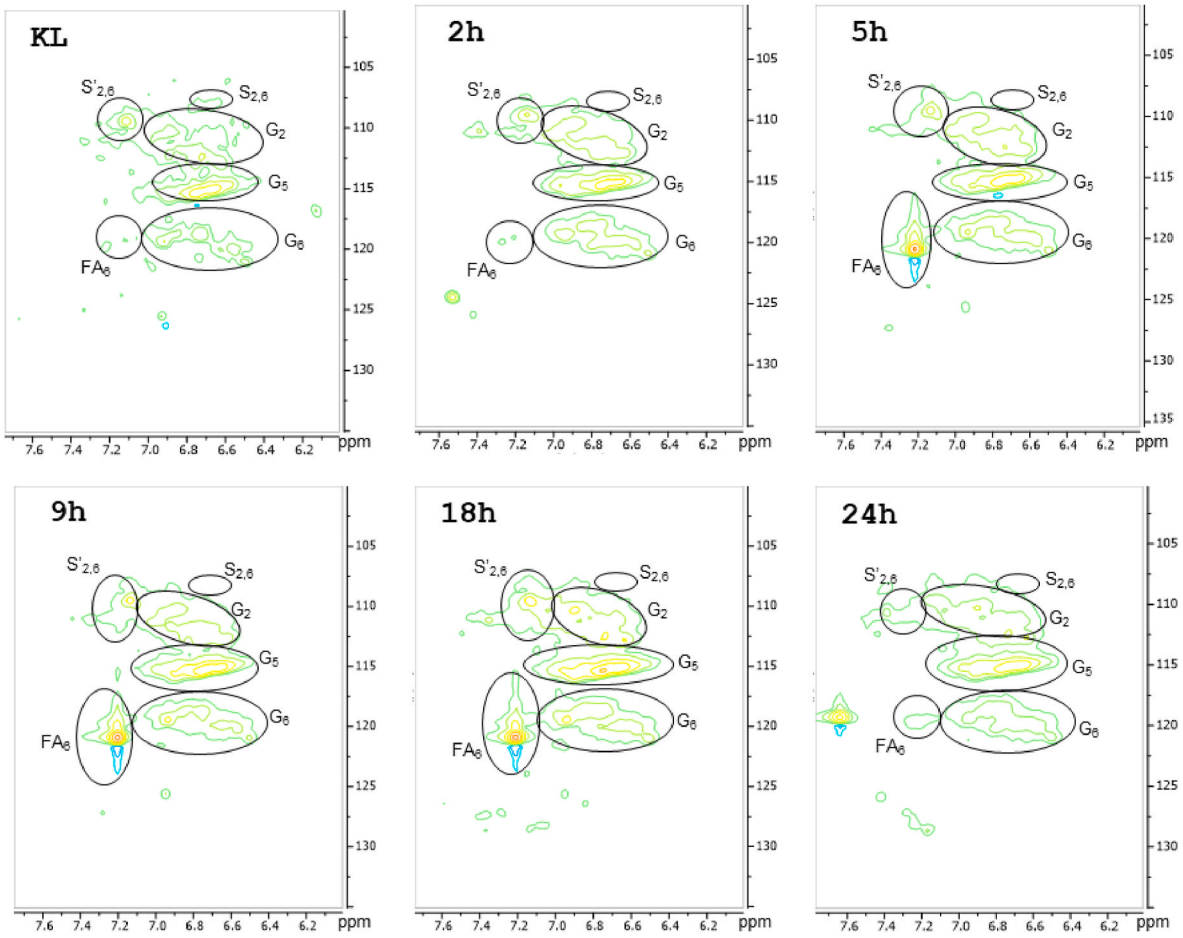

Fig. 3. Aromatic region in the 2D HSQC NMR spectra of kraft lignin and silylated samples as a function of reaction time.

suggesting that it depends on the reaction time, in which the S units are selectively activated and modified according to the availability of reactive sites, demonstrating a reversibility process in which the silyl groups are initially incorporated and then undergo reorganizations or even possible recoil processes. In contrast, the $S_{2,6}$ signal disappears in the silylated samples, indicating that the sites corresponding to these positions are completely modified or blocked by the reaction. Regarding the guaiacyl units, the values of G_2 and G_5 remain relatively stable throughout the process, indicating that these positions are less susceptible to modification, while G_6 shows a pronounced increase up to 9 h and then decreases. This behavior suggests that although most guaiacyl units remain stable, some specific sites exhibit transient reactivity, which could be related to the transient incorporation of silyl groups followed by structural reorganization [41]. Finally, the FA_2 group shows a sharp increase from 0.2 to 2.7 in the first 2 h, together with oscillatory behavior. Furthermore, the FA_6 signal, which is associated with the formation of new phenolic groups or derivatives, shows a drastic behavior, starting from a very low value in unmodified lignin and increasing abruptly up to 9 h, then decreasing as the reaction time increases. This trend shows that the reaction initially induces the formation of highly functionalized sites in the aromatic fraction, which over time are affected by condensation or rearrangement processes that reduce their availability.

On the other hand, in the non-oxygenated aliphatic region (see Fig. 4), the incorporation of the TBDMS group is evident from the appearance of signals identified as SitBu and $SiMe_2$, which are not detected in unmodified lignin. The SitBu signal appears at 2 h with a value of 463.2, reaches a maximum at 5 h and then drops significantly. Similarly, the signal associated with the methyls of the incoming group ($SiMe_2$) increases up 5 h and then decreases with longer reaction times. This behavior indicates that the incorporation of the silylating agent is more efficient in the range up to 5 h, the moment when the maximum levels of silylation are reached, suggesting that the incorporation of functional groups such as silanes occurs rapidly in the first hours, while the functionalization slows down over time, which could be due to the lower availability of free hydroxyl groups to react at later times [42]. In fact, longer times may cause secondary processes such as partial hydrolysis of TBDMS groups or internal rearrangements [43].

^{1}H–^{13}C HSQC 2D NMR and FTIR spectroscopy findings confirm that the lignin modification was successfully carried out. Moreover, the impact of reaction time on the degree of chemical modification of lignin was also demonstrated. Fig. 5 shows a comparison of the results obtained by both techniques. For this purpose, the sum transmittance ratio for the new silylated bands (peaks at 838 and 779 cm^{-1}) of FTIR spectra was normalized to the band at 1510 cm^{-1} corresponding to the aromatic skeletal vibrations of the C–C bonds. This band remains clearly defined in both neat and silylated lignin and is therefore suitable for normalization. While, the sum area ratio for the silylated areas of HSQC was normalized to the G_2 area. As can be observed, both techniques display comparable results, since the evolution of the curves have a qualitatively similar evolution. This behavior suggests that the incorporation of the silylating agent is more efficient within the first 5 h, the point at which the maximum levels of silylation are achieved. This implies that the incorporation of functional groups such as silanes occurs rapidly in the initial hours. However, as the reaction continues for longer periods, secondary processes may take place, such as condensation, partial hydrolysis of the TBDMS groups, or internal rearrangements, all of which contribute to a reduction in the chemical modification. In this regard,

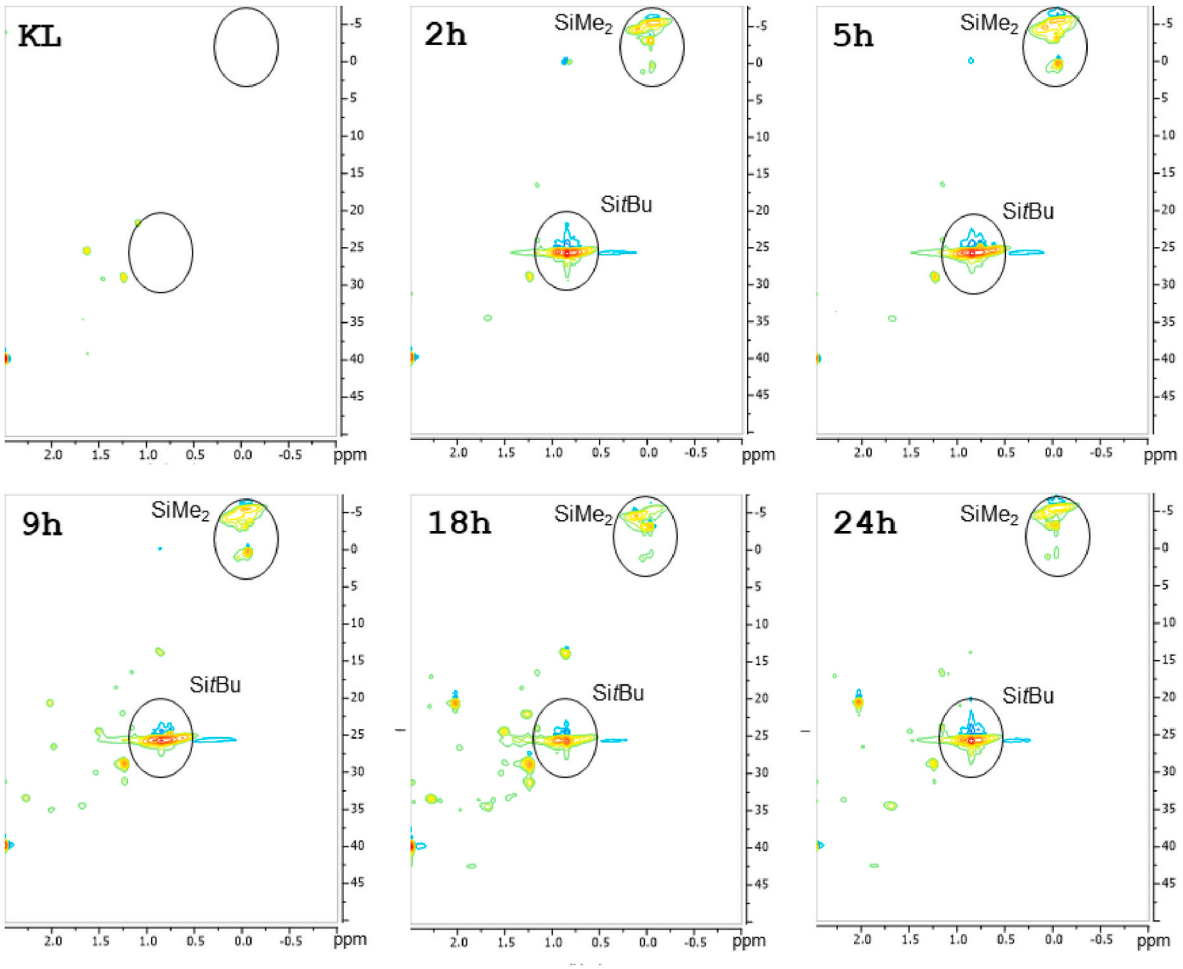

Fig. 4. Non-oxygenated aliphatic region in the 2D HSQC NMR spectra of kraft lignin and silylated samples as a function of reaction time.

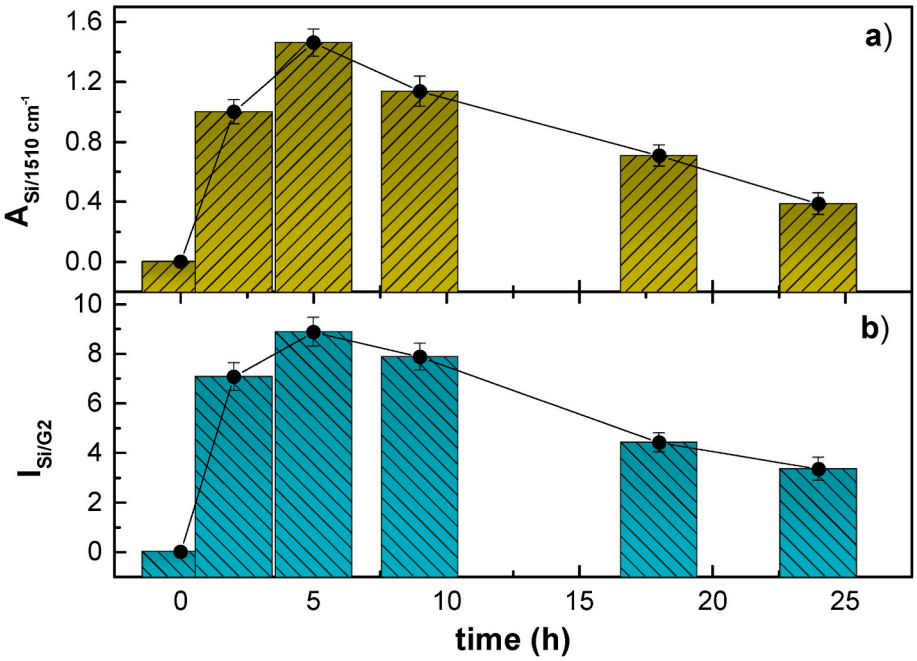

Fig. 5. Evolution of: (a) sum transmittance ratio of the silylated bands of FTIR spectra ($A_{Si/1510\ cm\text{-}1}$); (b) sum integral ratio of the silylated areas of HSQC (I_{Si}/I_{G2}) as a function of reaction time.

the decrease in signals associated with aliphatic silylation over prolonged reaction times could be associated with the lower stability of aliphatic Si–O bonds compared with the more stable aromatic Si–O–Ar bonds. Similarly, previous studies on the phenolation of lignin have shown that extending the reaction time results in a decrease in the extent of chemical modification [44].

Solubility tests were also carried out to assess the affinity between the samples and solvents of different polarities. As can be seen in Fig. 6a, the most of the neat lignin was present in the water fraction, as indicated by the region below the discontinuous line in the vial shown in this Figure. Some fractions of the samples were observed to settle at the bottom of the vial, as expected due to the hydrophilic nature of lignin. In addition, a meniscus was visible in all samples containing lignin fractions, a result of the surface tension of water and the cohesive forces between the water and the glass. Modified lignin fractions were not found in the water phase, indicating their hydrophobicity. While the sample modified with the longest reaction time (24 h) formed a stable layer at the toluene-water interface, the other samples were only dispersed in toluene, showing no dispersion in the water. This behavior can be attributed to the replacement of hydroxyl groups by silane groups

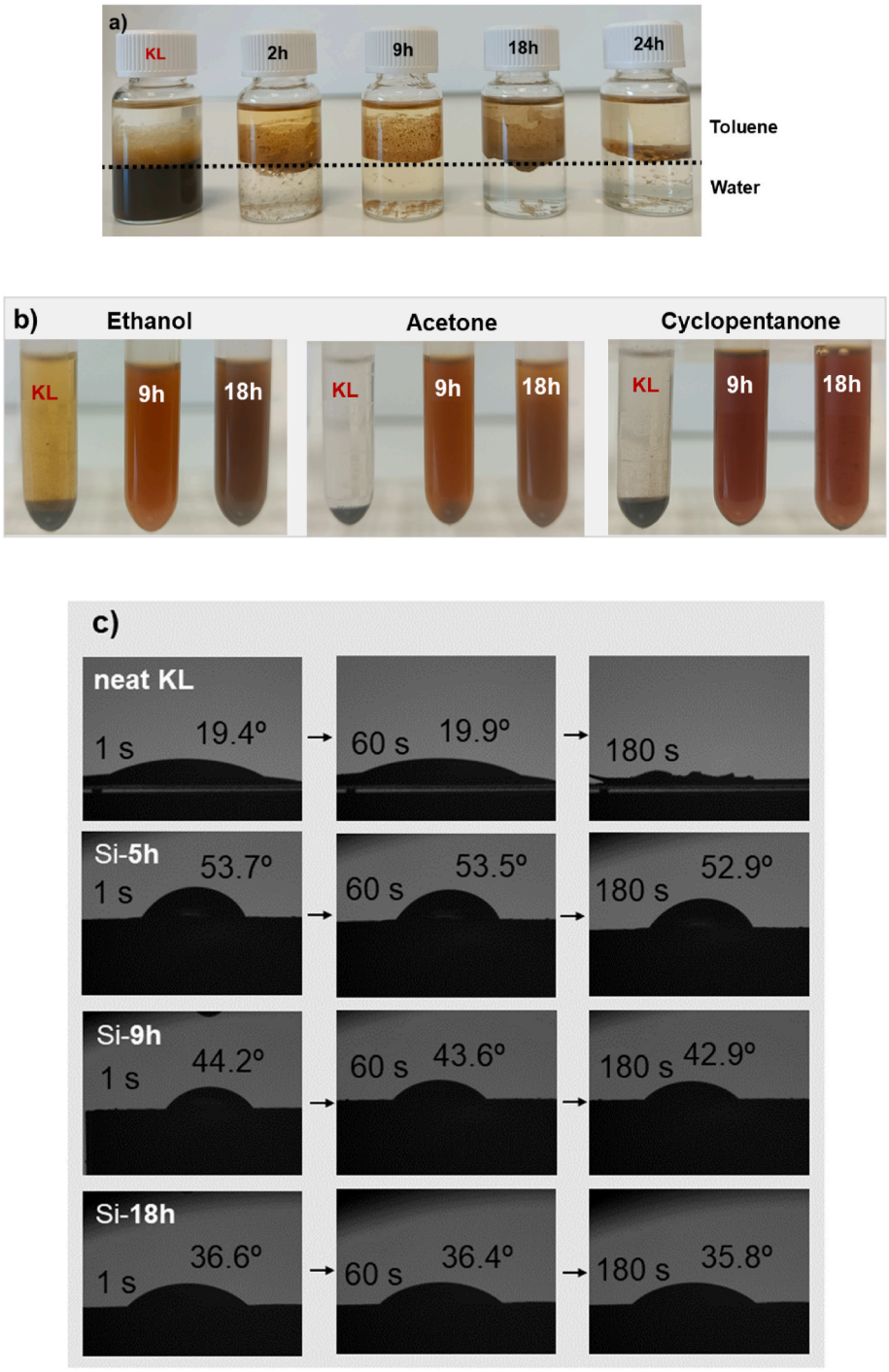

Fig. 6. (a) Solubility tests of KL and silylated samples in 1:1 (v/v) ratio of water (relative polarity - 1.0) and toluene (relative polarity – 0.099) mixture as a function of reaction time. (b) Appearance of KL and silylated samples in different organic solvents. (c) Water contact angles of neat KL and silylated samples as a function of reaction time.

in KL through silylation reaction. Although, the samples modified with the longest reaction times were also present at the toluene/water interface, confirming balanced hydrophobic and polar characteristics of these samples. In short, the KL exhibited a high hydrophilicity compared to the silylated lignin, which displayed different levels of hydrophobicity based on the extent of chemical modification. Other solvents such as ethanol, acetone and cyclopentanone were also chosen to evaluate the solubility of the samples. The appearance of the solubility of the samples in these organic solvents is shown in Fig. 6b. As can be seen, the pure lignin precipitated in all solvents. However, the silylated samples dissolved almost completely in these organic solvents, with cyclopentanone showing a slightly better solubility. Contact angles were also measured 1, 60 and 180 s after the water drop was applied to the sample surface in order to point out the effect of silylation process on the hydrophobic behavior of the lignin particles (see Fig. 6c). As expected, the resulting contact angle values obtained for the modified lignin samples were higher than those found for the neat KL. As can be observed at 180 s, the unmodified lignin particle absorbs the drop and the contact angle reduces to 0 since the abundance of hydroxyl groups in the lignin structure imparts a highly hydrophilic character. Furthermore, the water contact angle increased with the degree of substitution due to the replacement of surface hydroxyl groups with silane groups, which decreased the polarity of the lignin particles. Therefore, the sample with the highest contact angle is the modified sample with a reaction time of 5 h, as corroborated by the 2D HSQC NMR results. These results show that silylation changed the surface properties of the lignin particles from hydrophilic to more hydrophobic, which are in agreement with previous results [28,45].

Additionally, a morphological analysis was performed using scanning electron microscopy (SEM) to assess the changes in size and shape of lignin particles as a result of the silylation process, as a function of the reaction time. In this context, Fig. 7 presents selected scanning electron microscope (SEM) images of both KL and silylated samples. As observed, the powder of KL consists of wrinkled, irregular spherical granules or particles (Fig. 7a), while the silylated samples exhibit porous particles with pores scattered across their surfaces. Moreover, it was found that the particle size decreases significantly as the reaction time increases. In this regard, the morphology of the sample silylated 24 h stands out, showing a marked difference with agglomerates of micro- and nano-sized particles that are noticeably smaller than those found in the other samples (Fig. 7e). These results suggest that the silylation reaction may promote the supramolecular aggregation of lignin, initially forming clusters that evolve into micro- and nano-sized particles. In fact, the structure and functional groups of lignin significantly influence the formation and stability of lignin particles [46]. As shown by Wang et al., high molecular weight Kraft lignin, such as that used in this work, tends to form more uniform and smaller-sized lignin nanoparticles compared to low molecular weight fractions [47]. This can be ascribed to the fact that high molecular weight (and more condensed) fractions promote the self-assembly through hydrophobic interactions, such as π−π stacking, whereas low molecular weight fractions contain relatively high amounts of hydroxyl groups that hinder such interactions and thus prevent the packing of lignin during the self-assembly.

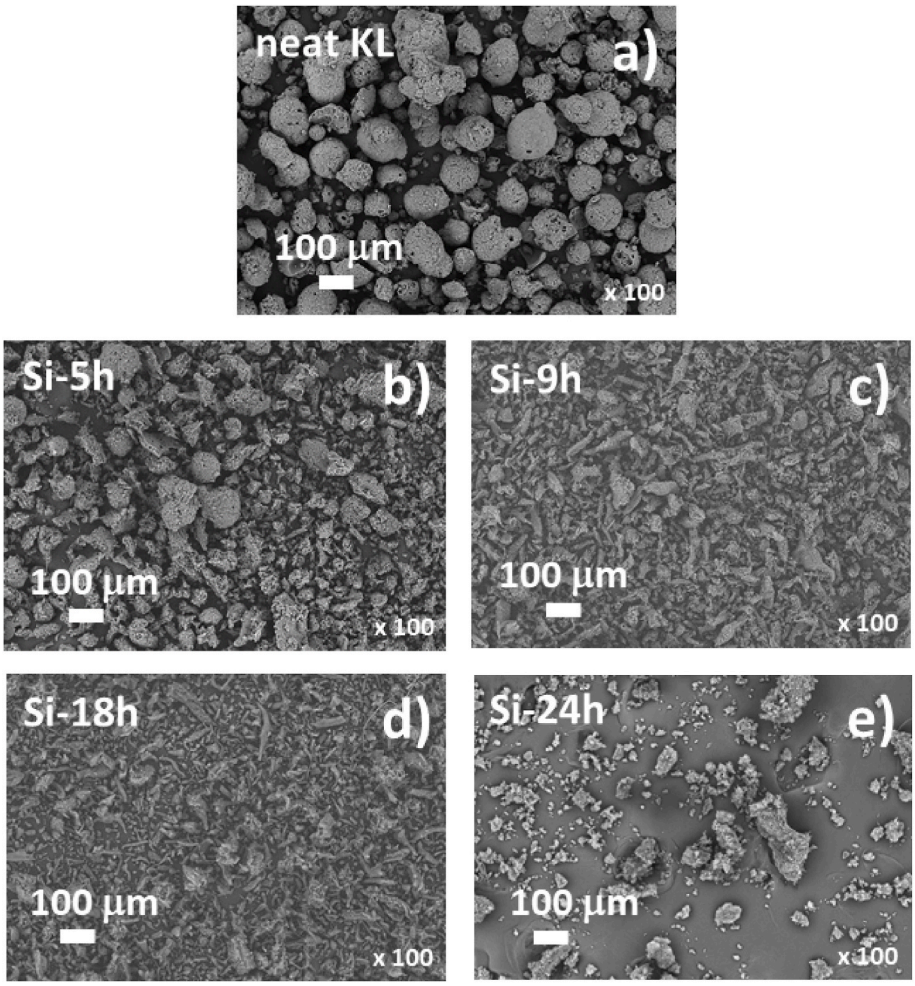

Fig. 7. SEM micrographs of selected samples: (a) neat KL, (b) silylated 5 h, (c) silylated 9 h, (d) silylated 18 h, (e) silylated 24 h.

3.2. Influence of the silylation process on the rheological and tribological properties of the oleo-dispersions

From a rheological point of view, the development of oleo-dispersion formulations requires the characterization of both viscous flow and linear viscoelastic properties. This is essential to provide the basis for a more detailed explanation of the interaction between the different components in the dispersion, as well as a better basis for the physicochemical modification of lignin and the control of rheological properties. Fig. 8a shows oleo-dispersion viscous flow curves as a function of silylation reaction time. Castor oil was included for the sake of comparison. For castor oil a Newtonian behavior was observed, i.e. a constant value of viscosity over the range of shear rates studied. On the contrary, all the oleo dispersions showed a shear thinning behavior and, as can be observed, both the viscosity and the shear rate dependence (non-Newtonian behavior) increase with the silylation reaction time. The viscous flow properties of these materials may be linked to the volume fraction of the dispersed phase, which can be influenced by physical and/or chemical interactions between the lignin molecules and the oil medium. In this regard, the different viscosity values observed, particularly at low shear rates for the oleo-dispersions, indicate that the developed colloidal network is likely to be significantly different. In this sense, frequency sweep tests can provide further insight into the effect of silylation on the colloidal network formed by silylated lignins in the oleo-dispersions. Fig. 8b shows the evolution of SAOS functions with frequency, within the linear viscoelastic range, as a function of silylation reaction time. As can be observed, the oleo-dispersions exhibit a variety of viscoelastic behaviors as the oleo-dispersion undergoes a liquid–gel transition (LGT) due to changes in the physicochemical properties of the lignin, as shown by the evolution of G' and G" with the angular frequency. A viscoelastic liquid-like response was observed at low reaction times (2 and 5 h) where G" > G', with both moduli having a near-linear dependence on frequency. For an intermediate reaction time (9 h), oleo-dispersion shows that G' and G" curves intersect at an intermediate frequency, suggesting a clear tendency to form a soft gel. Whereas at high reaction times (16, 18 and 24 h), G' > G" over a wide frequency range, evincing a stronger viscoelastic gel-like behavior and the formation of remarkably stable colloid-lignin network. These findings show that the silylation process has a significant impact on the rheological properties of the oleo-dispersions and can modulate the physicochemical interactions between the lignin particles and the castor oil. This phase (liquid–gel) transition of oleo-dispersions is better illustrated using the Han–Chuang plot (Fig. 8c), where the storage modulus (G') is plotted versus the loss modulus (G"). On double-logarithmic scales, the equimoduli line (G' = G", slope = 1) represents the liquid–gel transition, i.e. a critical gel viscoelastic behavior, and was included to guide data interpretation. Regions above this line indicate gel-like behavior, whereas regions below correspond to liquid-like behavior. As shown in Fig. 8c, the sample processed for 9 h is representative of the transition from liquid-like to gel-like behavior, with G' exceeding G" at longer

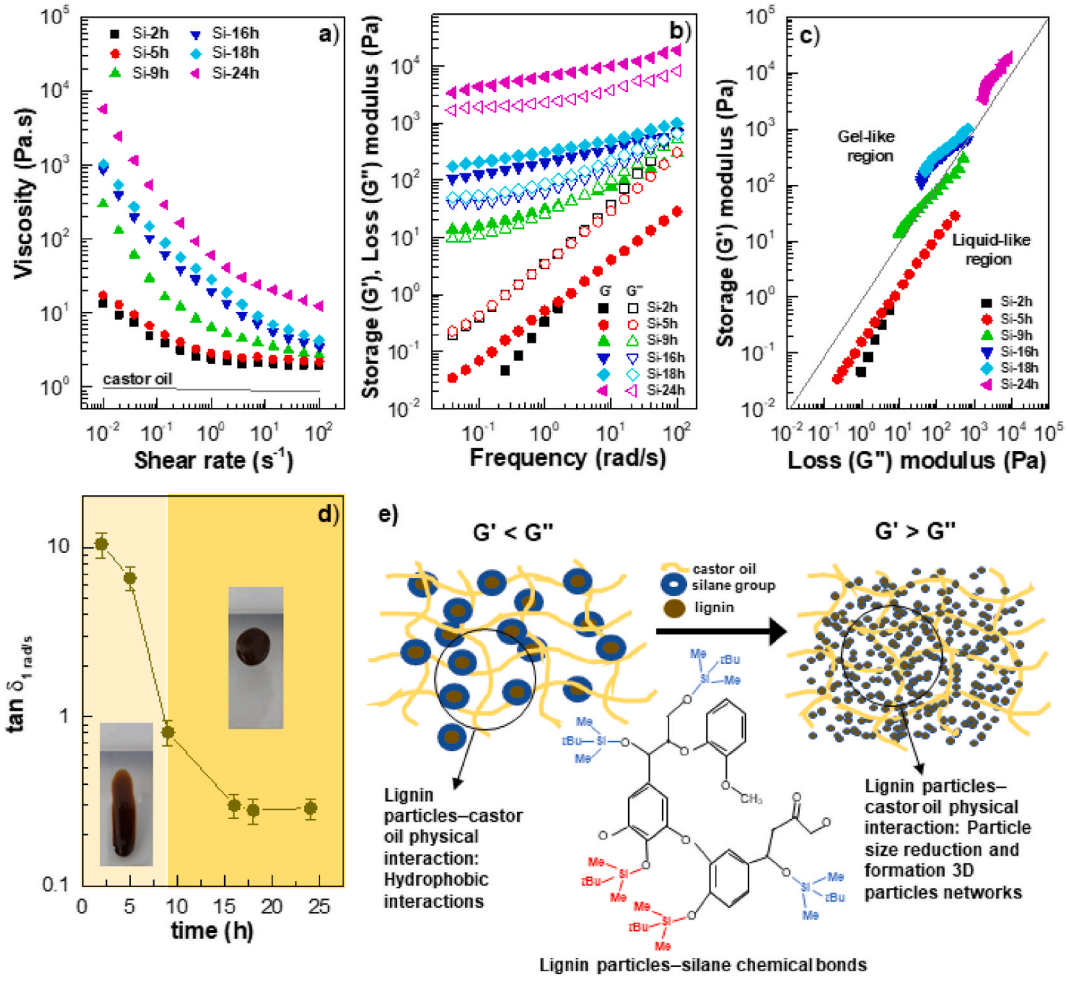

Fig. 8. (a) Viscous flow curves of oleo-dispersions as a function of reaction time. (b) Viscoelastic properties of oleo-dispersions formulated with silylated samples as a function of reaction time. (c) Storage modulus vs. loss modulus plots of oleo-dispersions formulated with silylated samples as a function of reaction time. (d) tan δ at 1 rad/s of oleo-dispersions as a function of reaction time. (e) Proposed scheme of microstructures and transition from a viscoelastic liquid-like behavior to solid-like gel behavior of the oleo-dispersions.

reaction times, confirming gel formation. In the same way, the loss tangent, tan(δ) = G"/G', plotted at 1 rad/s versus reaction time (Fig. 8d), identifies the onset of the phase transition at tan(δ) = 1, again providing an estimation of a minimum silylation time of ~9 h for the formation of a gel network. The rheological results obtained suggest that the colloidal network formed in the oleo-dispersions could be attributed to the balance of repulsive/attractive forces between the lignin particles and the castor oil due to the physicochemical modification induced by the silylation process. On the one hand, the hydrophobic/hydrophilic properties of lignin can be adjusted by chemical modification. The addition of the silane group, which imparts a strong hydrophobic character to the lignin particles, acts as a 'bridge' for interaction with castor oil, enhancing compatibility and dispersibility with the oil. This does not result in a significant increase in the viscosity or any thickening effect in the base oil, as demonstrated by the sample processed for 5 h, which exhibits the greatest chemical modification with silane groups. However, after 5 h, a significant increase in castor oil viscosity occurs, showing a more pronounced non-Newtonian character, with a clear tendency to reach a high-shear-rate-limiting viscosity. Therefore, the viscous flow behaviour of these materials is related to the balance between physical, i.e. changes in the volume fraction of the dispersed phase, and chemical (hydrophobic) interactions between lignin molecules and the oil medium. Of course, the silylation process alters the area/volume ratio of lignin particles, particularly increasing with silylation time (as shown in the SEM micrographs), which in turn increases the effective volume fraction in the oleo-dispersion. This facilitates the formation of percolating network structures of lignin particles. At low reaction times (2 and 5 h) the highest levels of chemical modification were achieved (lignin particles with a strong hydrophobic character), while lower levels of physical modification were observed. As a result,

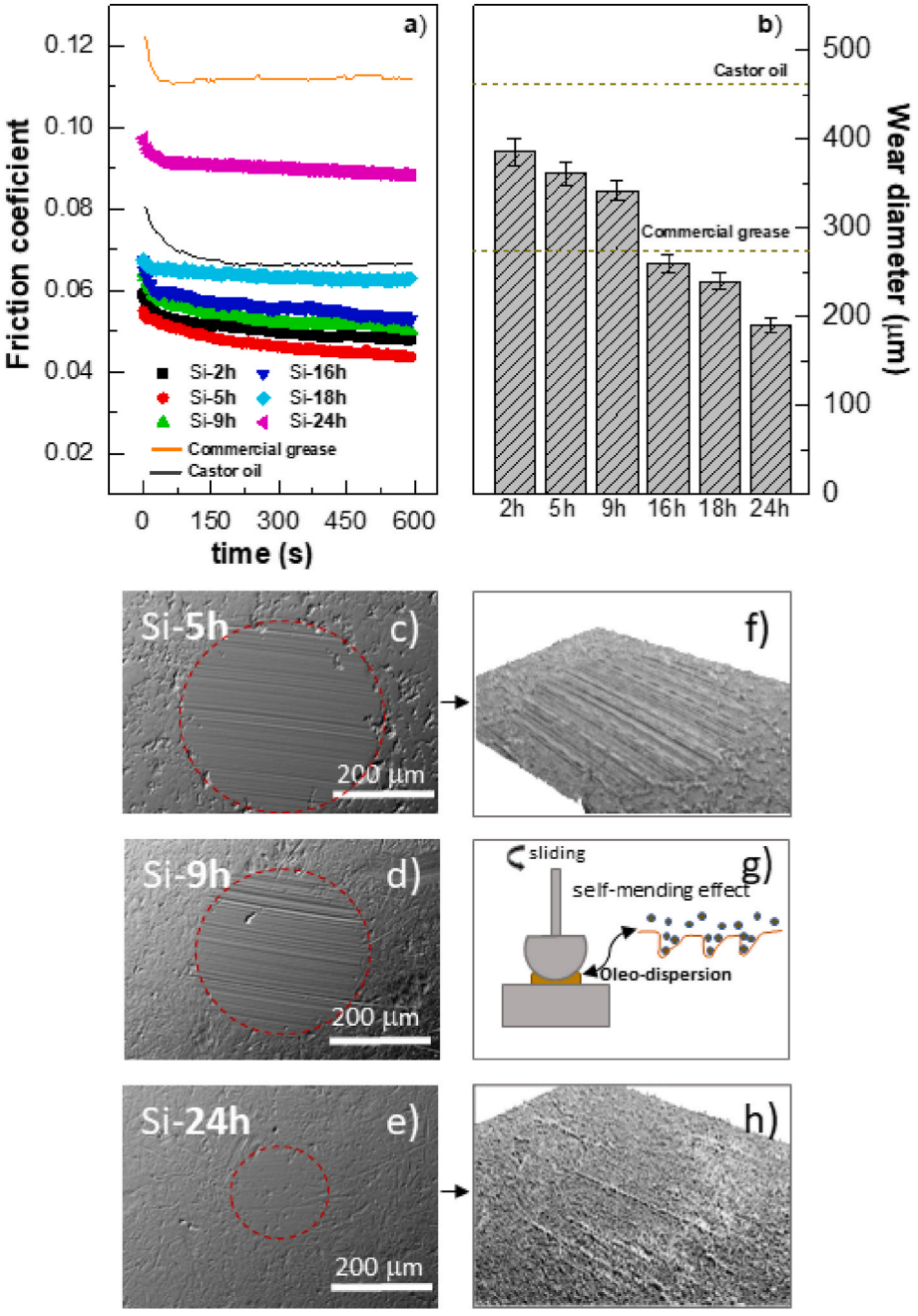

Fig. 9. (a) Friction curves for oleo-dispersions as a function of reaction time. (b) Wear diameter as a function of reaction time. (c, d, e) Selected SEM images of wear scars for oleo-dispersions as a function of reaction time. (g) Proposed scheme of lubricating mechanism for oleo-dispersions.

the oleo dispersions showed a viscoelastic liquid-like behaviour ($G' < G''$), as a result of the higher compatibility with the castor oil. In this sense, as above discussed, the highly modified lignin samples present a higher solvency for the castor oil, understood the thickener's solvency as the ability to dissolve and/or disperse properly in a specific medium. However, at longer reaction times (16, 18 and 24 h) the situation was reversed. Lignin particles with intermediate hydrophobic/hydrophilic properties, i.e. lower solvency, and high area/volume ratios, facilitating the formation of percolating network structures. This resulted in a viscoelastic gel-like behaviour ($G' > G''$). These mechanisms have been illustrated in Fig. 8e, which shows a proposed scheme for the transition from a viscoelastic liquid-like behavior to solid-like behavior in these of oleo-dispersions, depending on the sylilation degree.

The lubrication properties of the oleo-dispersions were investigated in a ball-on-plate tribological contact. Specific normal load (20 N) and rotational speed (100 rpm) conditions were selected to compare the results with those obtained in a previous work [7], where modified lignin dispersions were formulated using esterification reactions. Fig. 9a presents the coefficient of friction (CoF) versus sliding time for the oleo-dispersions as a function of the silylation reaction time, castor oil and a lithium lubricating grease. It can be observed from the figure that for all the samples, the CoF decreases to a stable value at around 600 s, with some fluctuations in the CoF values for the oleo-dispersion with the longest silylation time. The initially higher CoF values can be attributed to the formation of the tribofilm. As reported by several authors [48,49], the creation of tribofilms increases surface roughness, which in turn leads to an increase in CoF, slows down the micro-elastohydrodynamic lubrication effects, and thus results in a higher CoF [50]. Most remarkably, Fig. 9a shows that high sylilation levels results in a significant reduction of CoF values, whereas friction increases with longer silylation times. This behavior may be due to the rheological properties of the oleo dispersions; it is known that a reduced effective viscosity favors the replenishment of the friction track more efficiently [51,52]. Interestingly, the CoF values obtained for both the liquid-like and gel-like dispersions were lower than those obtained for castor oil and a commercial lithium grease. Fig. 9c–e presents the SEM micrographs of the worn surfaces of the steel plates lubricated by using the oleo-dispersions as a function of silylation time. A wear mark appears and linear grooves in the sliding direction are seen in the plates after the friction test. As can be seen, the wear mark decreases as the silylation time increases (see Fig. 9b). Based on these results, it can be suggested that when lubricated with oleo-dispersions, particularly the gel-like dispersions, a protective surface layer composed of silylated lignin particles and oil molecules forms at the interface of the friction pair. This layer helps to prevent direct contact between the ball and the steel plate, effectively reducing wear. Tribochemical reactions, polishing or rolling effects, or a mixture of these, are often proposed as tribological mechanisms to explain the formation of a protective surface layer when friction occurs [53]. A key explanation in this case is that lignin particles help to fill in the grooves and scars on the friction surface, compensating for mass loss by a process called self-mending (Fig. 9g). This mechanism is supported by the fact that surfaces lubricated with gel-like dispersions tend to be less worn than those lubricated with liquid-like dispersions (see 3D images in Fig. 9f and h). A similar mechanism has been proposed for oleo-dispersions of cellulose nanocrystals in polyalphaolefin oil, as well as for oleo-dispersions formulated with silylated cellulose pulp and castor oil [54,55]. On the other hand, it is likely that the silane groups present in the dispersions adsorb onto the steel interface, initiating tribochemical reactions between iron (Fe), silicon (Si), and oxygen (O). These reactions are promoted by the frictional forces and the heat generated during the process. As a result, a chemical transfer film made up of iron and silicon oxides forms, which has been shown to offer high resistance to both friction and wear [56,57].

4. Conclusions

In this work, we demonstrated that a straightforward silylation route can be employed as a powerful tool to modulate the rheological and tribological properties of oleo-dispersions based on lignin for the development of environmentally friendly lubricants. Lignin sylilation was successfully modulated by controlling the reaction with tert-butyldimethylsilyl chloride (TBDMSCl), in the presence of dimethylformamide and imidazole as the solvent and catalyst, respectively, as a function of the reaction time. It was found that the incorporation of the silylating agent was most efficient within the first 5 h, after which secondary processes such as condensation, partial hydrolysis, or internal rearrangements could occur, all contributing to a reduction in chemical modification, but an increase of the physical modification. Fine dispersions of sylilated lignins in castor oil exhibited two different rheological behaviors depending on the reaction time: shorter reaction times (2-5 h) resulted in oleo-dispersions with liquid-like properties, while longer reaction times (16-24 h) produced dispersions with a mechanical spectrum characteristic of particle networks, typical of solid gel-like materials. This distinct behavior was attributed to the different compatibility or solvency between the lignin particles and the vegetable oil, favoured by high levels of sylilation, and changes in physical properties such as size, morphology, and surface of the lignin particles, favoured by high reaction times. In terms of lubricity, the oleo-dispersions of sylilated lignins showed excellent friction and wear performance in the mixed lubrication regime, comparable to or better than (lignin-free) castor oil or conventional lithium lubricating greases, due to the mending effect of the silylated lignin particles on surface roughness and scars. Overall, this work represents a significant advance in the development of sustainable structuring agents derived from low-cost polymeric materials like lignin, offering a fast and straightforward approach with particular relevance to applications in the lubricant industry.

CRediT authorship contribution statement

M. Trejo-Cáceres: Writing – original draft, Validation, Methodology, Investigation, Formal analysis, Data curation, Conceptualization. **J. E. Martín-Alfonso:** Writing – review & editing, Writing – original draft, Visualization, Validation, Supervision, Resources, Project administration, Methodology, Investigation, Funding acquisition, Formal analysis, Data curation, Conceptualization. **J.M. Franco:** Writing – review & editing, Validation, Supervision, Resources, Project administration, Methodology, Investigation, Funding acquisition, Conceptualization.

Declaration of competing interest

The authors declare that they have no known competing financial interests or personal relationships that could have appeared to influence the work reported in this paper.

Acknowledgments

This work is part of the Research Projects PID2021-125637OB-I00 and PID2024-159052OB-I00, funded by MICIU/AEI/10.13039/501100011033 and by ERDF/EU and project Ref. 802C1800001, cofunded by ERDF/EU (80%) and Junta de Andalucía (Consejería de Economía, Conocimiento, Empresas y Universidades/Agencia-IDEA). Funding is gratefully acknowledged. Funding for open access charge: Universidad de Huelva/CBUA.

Appendix A. Supplementary data

Supplementary data to this article can be found online at https://doi.org/10.1016/j.polymer.2026.129769.

Data availability

Data will be made available on request.

References

[1] L. Huo, J. Guo, F. Yang, C. Pan, H. Hu, K. Zhang, H. Zhou, P. Liu, Design of linear polymer-based liquid lubricants by a strategy of complementary advantages, Polymer (Guildf). 265 (2023) 125592, https://doi.org/10.1016/j.polymer.2022.125592.

[2] S. Liu, Q. Gao, K. Hou, Z. Li, J. Wang, S. Yang, Solvent-free covalent MXene nanofluid: a new lubricant combining the characteristics of solid and liquid lubricants, Chem. Eng. J. 462 (2023) 142238, https://doi.org/10.1016/j.cej.2023.142238.

[3] K. Holmberg, A. Erdemir, The impact of tribology on energy use and CO2 emission globally and in combustion engine and electric cars, Tribol. Int. 135 (2019) 389–396, https://doi.org/10.1016/j.triboint.2019.03.024.

[4] S.K. Yeong, P.F. Luckham, ThF. Tadros, Steady flow and viscoelastic properties of lubricating grease containing various thickener concentrations, J. Colloid Interface Sci. 274 (2004) 285–293, https://doi.org/10.1016/j.jcis.2004.02.054.

[5] J.E. Martín-Alfonso, A. Romero, C. Valencia, J.M. Franco, Formulation and processing of virgin and recycled polyolefin/oil blends for the development of lubricating greases, J. Ind. Eng. Chem. 19 (2013) 580–588, https://doi.org/10.1016/j.jiec.2012.09.012.

[6] A. Saxena, D. Kumar, N. Tandon, Development of eco-friendly nano-greases based on vegetable oil: an exploration of the character via structure, Ind. Crops Prod. 172 (2021) 114033, https://doi.org/10.1016/j.indcrop.2021.114033.

[7] M. Trejo-Cáceres, M.C. Sánchez, J.E. Martín-Alfonso, Impact of acetylation process of kraft lignin in development of environment-friendly semisolid lubricants, Int. J. Biol. Macromol. 227 (2023) 673–684, https://doi.org/10.1016/j.ijbiomac.2022.12.096.

[8] Z. Wu, P.P. Thoresen, L. Matsakas, U. Rova, P. Christakopoulos, Y. Shi, Facile synthesis of lignin-castor oil-based oleogels as green lubricating greases with excellent lubricating and antioxidation properties, ACS Sustain. Chem. Eng. (2023), https://doi.org/10.1021/acssuschemeng.3c01801.

[9] E. Cortés-Triviño, C. Valencia, M.A. Delgado, J.M. Franco, Modification of Alkali Lignin with Poly(Ethylene glycol) diglycidyl ether to be used as a thickener in bio-lubricant formulations, Polymers (Basel) 10 (2018) 670, https://doi.org/10.3390/polym10060670.

[10] J. Zhang, D. Cao, B. Chen, Y. Huang, L. Huang, X. Feng, J. Zhu, X. Lu, L. Mu, Controlling lignin solubility in nonpolar lubricating oil via multiple fatty chains modification strategy, ACS Sustain. Chem. Eng. 12 (2024) 12744–12754, https://doi.org/10.1021/acssuschemeng.4c02149.

[11] M.A. Jedrzejczyk, S. Van den Bosch, J. Van Aelst, K. Van Aelst, P.D. Kouris, M. Moalin, G.R.M.M. Haenen, M.D. Boot, E.J.M. Hensen, B. Lagrain, B.F. Sels, K. V. Bernaerts, Lignin-based additives for improved thermo-oxidative stability of biolubricants, ACS Sustain. Chem. Eng. 9 (2021) 12548–12559, https://doi.org/10.1021/acssuschemeng.1c02799.

[12] L. Mu, Y. Shi, X. Guo, J. Wu, T. Ji, L. Chen, X. Feng, X. Lu, J. Hua, J. Zhu, Enriching heteroelements in lignin as lubricating additives for bioionic liquids, ACS Sustain. Chem. Eng. 4 (2016) 3877–3887, https://doi.org/10.1021/acssuschemeng.6b00669.

[13] X. Ren, X. Zhang, Q. Zhang, L. Chen, J. Liu, L. Ma, Preparation and characterization of lignin-phenol-formaldehyde resins using the lignin derived from various biorefinery processes, Polymer (Guildf). 335 (2025) 128788, https://doi.org/10.1016/j.polymer.2025.128788.

[14] A.F. Tiniakos, C. Samiotaki, A. Zamboulis, A. Grigoropoulos, S. Koutsourea, E. Tarani, A. Teknetzi, G. Vourlias, A. Zoikis Karathanasis, D.N. Bikiaris, I. Deligkiozi, Investigating HDPE composites with Phosphorus- and Nitrogen-modified lignins, Polymer (Guildf). (2025) 129495, https://doi.org/10.1016/j.polymer.2025.129495.

[15] S. Roy, B. Godbole, N.R. Shiju, P. Biswas, Advanced lignin extraction technologies from diverse lignocellulosic biomass sources for modern biorefineries: a review, Mater. Today Chem. 47 (2025) 102826, https://doi.org/10.1016/j.mtchem.2025.102826.

[16] J. Tanks, T. Akagawa, K. Tamura, Y. Nemoto, K. Naito, Y. Watanabe, T.T. Nge, T. Yamada, Enhancing the thermo-oxidative stability of polyamide 6 by scalable melt-blending with PEG-grafted glycol lignin, Polymer (Guildf). 335 (2025) 128853, https://doi.org/10.1016/j.polymer.2025.128853.

[17] Z. Wang, Q. Gao, Y. Zhou, Y. Xu, T. Hong, L. Shu, Fabrication of dealkalized-lignin/polyacrylonitrile based carbon fiber via dry-jet wet spinning process, Polymer (Guildf). 340 (2025) 129266, https://doi.org/10.1016/j.polymer.2025.129266.

[18] X. Zhen, X. Cui, A.A.N.M. Al-Haimi, Z. Xu, L. Li, M. Sun, J. Dong, X. Wang, Z. Jiang, Z. Wang, Lignin-based epoxy resins: understanding the impact of hydrogenolysis oil composition, Polymer (Guildf). 342 (2026) 129359, https://doi.org/10.1016/j.polymer.2025.129359.

[19] J. Zhang, D. Cao, S. Wang, X. Feng, J. Zhu, X. Lu, L. Mu, Valorization of industrial lignin as lubricating additives by C–C bond cleavage and doping heteroelement-rich groups, Biomass Bioenergy 161 (2022) 106470, https://doi.org/10.1016/j.biombioe.2022.106470.

[20] E. Cortés-Triviño, C. Valencia, J.M. Franco, Influence of epoxidation conditions on the rheological properties of gel-like dispersions of epoxidized kraft lignin in Castor oil, Holzforschung 71 (2017) 777–784, https://doi.org/10.1515/hf-2017-0012.

[21] A.M. Borrero-López, A. Blánquez, C. Valencia, M. Hernández, M.E. Arias, M. E. Eugenio, Ú. Fillat, J.M. Franco, Valorization of soda lignin from wheat straw solid-state fermentation: production of oleogels, ACS Sustain. Chem. Eng. 6 (2018) 5198–5205, https://doi.org/10.1021/acssuschemeng.7b04846.

[22] J. Gendron, I. Stambouli, C. Bruel, Y. Boumghar, D. Montplaisir, Characterization of different types of lignin and their potential use in green adhesives, Ind. Crops Prod. 182 (2022) 114893, https://doi.org/10.1016/j.indcrop.2022.114893.

[23] M.A. Martín-Alfonso, J.F. Rubio-Valle, J.P. Hinestroza, J.E. Martín-Alfonso, Impact of vegetable oil type on the rheological and tribological behavior of montmorillonite-based oleogels, Gels 8 (2022) 504, https://doi.org/10.3390/gels8080504.

[24] S. Su, F. Cao, S. Wang, Q. Shen, G. Luo, Q. Lu, G. Song, Organoborane-catalysed reductive depolymerisation of catechyl lignin under ambient conditions, Green Chem. 25 (2023) 8172–8180, https://doi.org/10.1039/D3GC02025H.

[25] A. Eraghi Kazzaz, Z. Hosseinpour Feizi, P. Fatehi, Grafting strategies for hydroxy groups of lignin for producing materials, Green Chem. 21 (2019) 5714–5752, https://doi.org/10.1039/C9GC02598G.

[26] B. Prieur, M. Meub, M. Wittemann, R. Klein, S. Bellayer, G. Fontaine, S. Bourbigot, Phosphorylation of lignin to flame retard acrylonitrile butadiene styrene (ABS), Polym. Degrad. Stabil. 127 (2016) 32–43, https://doi.org/10.1016/j.polymdegradstab.2016.01.015.

[27] G.L. Bykov, B.G. Ershov, A sorbent based on phosphorylated lignin, Russ. J. Appl. Chem. 83 (2010) 316–319, https://doi.org/10.1134/S1070427210020254.

[28] P. Buono, A. Duval, P. Verge, L. Averous, Y. Habibi, New insights on the chemical modification of Lignin: acetylation versus silylation, ACS Sustain. Chem. Eng. 4 (2016) 5212–5222, https://doi.org/10.1021/acssuschemeng.6b00903.

[29] J. Lv, T. Luo, D. Zou, H. Dong, Using DMF as both a catalyst and cosolvent for the regioselective silylation of polyols and diols, Eur. J. Org Chem. 2019 (2019) 6383–6395, https://doi.org/10.1002/ejoc.201901195.

[30] P. Patschinski, H. Zipse, Leaving group effects on the selectivity of the silylation of alcohols: the reactivity–selectivity principle revisited, Org. Lett. 17 (2015) 3318–3321, https://doi.org/10.1021/acs.orglett.5b01536.

[31] J. Lawandi, S. Rocheleau, N. Moitessier, Regioselective acylation, alkylation, silylation and glycosylation of monosaccharides, Tetrahedron 72 (2016) 6283–6319, https://doi.org/10.1016/j.tet.2016.08.019.

[32] T. Rashid, C.F. Kait, T. Murugesan, A "Fourier Transformed Infrared" compound study of lignin recovered from a formic acid process, Procedia Eng. 148 (2016) 1312–1319, https://doi.org/10.1016/j.proeng.2016.06.547.

[33] O. Faix, Classification of lignins from different botanical origins by FT-IR spectroscopy, Holzforschung 45 (1991) 21–28, https://doi.org/10.1515/hfsg.1991.45.s1.21.

[34] Z. Zhang, G. Sèbe, D. Rentsch, T. Zimmermann, P. Tingaut, Ultralightweight and flexible silylated nanocellulose sponges for the selective removal of oil from water, Chem. Mater. 26 (2014) 2659–2668, https://doi.org/10.1021/cm5004164.

[35] Z. Zhang, P. Tingaut, D. Rentsch, T. Zimmermann, G. Sèbe, Controlled silylation of nanofibrillated cellulose in water: reinforcement of a model polydimethylsiloxane network, ChemSusChem 8 (2015) 2681–2690, https://doi.org/10.1002/cssc.201500525.

[36] T. Xia, Y. Huang, P. Lan, L. Lan, N. Lin, Physical modification of cellulose nanocrystals with a synthesized triblock copolymer and rheological thickening in silicone oil/grease, Biomacromolecules 20 (2019) 4457–4465, https://doi.org/10.1021/acs.biomac.9b01186.

[37] D. Rigo, N. Kohlhuber, L. Fliri, D. Diment, M. Cho, I. Sumerskii, M. Hummel, A. Potthast, M. Balakshin, Upgrading AquaSolv Omni (AqSO) biorefinery: access to highly ethoxylated lignins in high yields through reactive extraction (REx), Green Chem. 26 (2024) 2623–2637, https://doi.org/10.1039/D3GC03776B.

[38] M.M. Abu-Omar, K. Barta, G.T. Beckham, J.S. Luterbacher, J. Ralph, R. Rinaldi, Y. Román-Leshkov, J.S.M. Samec, B.F. Sels, F. Wang, Guidelines for performing lignin-first biorefining, Energy Environ. Sci. 14 (2021) 262–292, https://doi.org/10.1039/D0EE02870C.

[39] G. Pavaneli, T.A. da Silva, S.F. Zawadzki, G.L. Sassaki, R.A. de Freitas, L.P. Ramos, Production of highly antioxidant lignin nanoparticles from a hardwood technical lignin, Int. J. Biol. Macromol. 257 (2024) 128612, https://doi.org/10.1016/j.ijbiomac.2023.128612.

[40] S. Wu, L. Wang, S. Li, Y. Wang, S. Lei, J. Tang, J. Cui, X. Bian, J. Jiang, Y. Zhang, Bio-inspired modification of nanocellulose based on in-situ homogeneous radical coupling of coniferin, Int. J. Biol. Macromol. 292 (2025) 139270, https://doi.org/10.1016/j.ijbiomac.2024.139270.

[41] A. Hoffmann, J.P. Nong, A. Porzel, M. Bremer, S. Fischer, Modification of Lignoboost Kraft Lignin from softwoods with dihydroxybenzenes, React. Funct. Polym. 142 (2019) 112–118, https://doi.org/10.1016/j.reactfunctpolym.2019.06.011.

[42] T.E. Leventis, P. Judge, J. Zhang, M.Z.H. Kazmi, M.B. Foston, F.J. Williams, Boron Lewis acid extraction of wood generates high quality lignin, ACS Sustain. Chem. Eng. 12 (2024) 17210–17221, https://doi.org/10.1021/acssuschemeng.4c06206.

[43] H. Mou, J. Huang, W. Li, X. Wu, Y. Liu, H. Fan, Study on the chemical modification of alkali lignin towards for cellulase adsorbent application, Int. J. Biol. Macromol. 149 (2020) 794–800, https://doi.org/10.1016/j.ijbiomac.2020.01.229.

[44] J. Ou, S. Li, W. Li, C. Liu, J. Ren, F. Yue, Revealing the structural influence on Lignin phenolation and its nanoparticle fabrication with tunable sizes, ACS Sustain. Chem. Eng. 10 (2022) 14845–14854, https://doi.org/10.1021/acssuschemeng.2c04701.

[45] R. Shorey, A. Gupta, T.H. Mekonnen, Hydrophobic modification of lignin for rubber composites, Ind. Crops Prod. 174 (2021) 114189, https://doi.org/10.1016/j.indcrop.2021.114189.

[46] A. Moreno, M. Hakkarainen, Lignin-based functional materials, Biomacromolecules 26 (2025) 5493–5496, https://doi.org/10.1021/acs.biomac.5c01546.
[47] Z. Wang, C. Li, X. Liu, W. Jia, L. Huang, L. Wu, H. Shi, Formation of homogeneous lignin nanoparticles from industrial kraft lignin via fractionation combined with antisolvent precipitation, Biomacromolecules 26 (2025) 1838–1849, https://doi.org/10.1021/acs.biomac.4c01604.
[48] A. Dorgham, A. Azam, A. Morina, A. Neville, On the transient decomposition and reaction kinetics of zinc dialkyldithiophosphate, ACS Appl. Mater. Interfaces 10 (2018) 44803–44814, https://doi.org/10.1021/acsami.8b08293.
[49] L. Taylor, A. Dratva, H.A. Spikes, Friction and wear behavior of zinc dialkyldithiophosphate additive, Tribol. Trans. 43 (2000) 469–479, https://doi.org/10.1080/10402000008982366.
[50] R. Yu, H. Liu, Q. Sun, W. Lou, S. Zhang, X. Wang, Y. Zhao, Experimental study on ZDDP tribofilm formation in grease lubricated rolling/sliding contacts, Tribol. Int. 206 (2025) 110594, https://doi.org/10.1016/j.triboint.2025.110594.
[51] B. Vengudusamy, C. Enekes, R. Spallek, On the film forming and friction behaviour of greases in rolling/sliding contacts, Tribol. Int. 129 (2019) 323–337, https://doi.org/10.1016/j.triboint.2018.08.026.
[52] P.M. Cann, Grease lubrication of rolling element bearings — role of the grease thickener, Lubric. Sci. 19 (2007) 183–196, https://doi.org/10.1002/ls.39.
[53] L. Kong, J. Sun, Y. Bao, Preparation, characterization and tribological mechanism of nanofluids, RSC Adv. 7 (2017) 12599–12609, https://doi.org/10.1039/C6RA28243A.
[54] M. Trejo-Cáceres, J.E. Martín-Alfonso, J.M. Franco, Silylation of wheat straw cellulose pulp for its valorization as rheology modifier of industrial hydrophobic fluids: cases of Castor oil and bitumen, Carbohydr. Polym. 364 (2025) 123778, https://doi.org/10.1016/j.carbpol.2025.123778.
[55] K. Li, X. Zhang, C. Du, J. Yang, B. Wu, Z. Guo, C. Dong, N. Lin, C. Yuan, Friction reduction and viscosity modification of cellulose nanocrystals as biolubricant additives in polyalphaolefin oil, Carbohydr. Polym. 220 (2019) 228–235, https://doi.org/10.1016/j.carbpol.2019.05.072.
[56] B. Zhang, Y. Xu, F. Gao, P. Shi, B. Xu, Y. Wu, Sliding friction and wear behaviors of surface-coated natural serpentine mineral powders as lubricant additive, Appl. Surf. Sci. 257 (2011) 2540–2549, https://doi.org/10.1016/j.apsusc.2010.10.019.
[57] B.-S. Zhang, B.-S. Xu, Y. Xu, F. Gao, P.-J. Shi, Y.-X. Wu, CU nanoparticles effect on the tribological properties of hydrosilicate powders as lubricant additive for steel–steel contacts, Tribol. Int. 44 (2011) 878–886, https://doi.org/10.1016/j.triboint.2011.03.002.